

Hyperon productions from Au+Au collisions at $\sqrt{s_{NN}}=200$ GeV.

Purabi Ghosh,¹ Sushant K. Singh,^{2,3} Santosh K. Agarwalla,¹ and Jajati K. Nayak^{4,*}

¹*Department of Applied Physics and Ballistics, Fakir Mohan University, Balasore-756019, India.*

²*Variable Energy Cyclotron Centre, 1/AF, Bidhan Nagar, Kolkata-700064, India*

³*HBNI, Training School Complex, Anushakti Nagar, Mumbai 400085, India*

⁴*Variable Energy Cyclotron Centre, 1/AF, Bidhan Nagar, Kolkata-700064, India*

(Dated: June 29, 2022)

We evaluate centrality dependence of hyperon, Λ , Ξ , Ω and K meson yields from Au+Au collisions at $\sqrt{s_{NN}}=200$ GeV using rate equation and compare with experimental observations. An increase in the yield per participating nucleon is observed with centrality. Higher rate of multistrange productions compared to single-strange are also observed in case of central collisions. Using rate equation or momentum integrated Boltzmann equation we discuss the yield microscopically which are then normalised with thermal pions to get the *yield ratio*, $(H_s + \bar{H}_s)/(\pi^+ + \pi^-)$ at various centralities. We have also evaluated the relative *yield of anti hyperons per participant* at various centralities and compared with observations made at RHIC. Increase in the rate of Ξ yield compared to Λ is realised in most central collisions. We find multi strange Ξ, Ω freeze-out at a temperature very close to T_c and Λ, K do little later.

I. INTRODUCTION

Strange hadrons are sensitive probes to understand the hot and dense medium formed in relativistic heavy ion collisions. Enhancement of strangeness productions in heavy ion central collisions relative to $p-p$ collisions was argued long back as a signal of quark gluon plasma formation [1, 2]. With similar argument the enhancement is supposed to increase with the increase in strangeness content of the hadron. This is why, the study on multi-strange baryons and their anti-particle productions in heavy-ion and $p-p$ collisions at Relativistic Heavy Ion Collider (RHIC) and Large Hadron Collider (LHC) are very much contemporary. Recently, the yield of Λ , Ξ , and Ω have been measured from both central and peripheral Au+Au collisions at $\sqrt{s_{NN}}=200$ GeV at midrapidity [3]. An increase in the yield of hyperons with number of participating nucleons, N_{part} is observed from peripheral to central collisions. The yield per participant (yield normalised with N_{part}) is also observed to increase gradually. The “*yield per participant*” is an important observable as it reflects the formation probability of a hadron from the bulk of the matter. This increase in *yield per participant* is more for multi-strange hyperons Ξ and Ω than the single strange hyperon Λ as reported in [3].

As the size of the colliding system increases, number of participants increases. This leads to more number of interactions and we observe an increase in the hadronic yield. But when we consider *yield per participant* as observable, then we try to remove the system size dependence. Then, it is expected that the *yield per participant* should go flat if the relationship between yield and N_{part} is linear. However, from the measurements of anti-hyperons, it is not observed [3]. *Yield per participant* is enhanced when we move from peripheral to central collisions. This indicates a non-linear dependence of yield with N_{part} . The rate of enhancement is more for multistrange baryons compared to single-strange baryons Λ .

Analogous to the above argument, another observable *yield ratio* $(H_s + \bar{H}_s)/(\pi^+ + \pi^-)$ provides similar observations from $Pb-Pb$ collisions at $\sqrt{s_{NN}}=2.76$ TeV. H_s , here, represents the yield of strange hadrons. In one of the recent measurements, ALICE Collaboration has reported the yield of strange mesons (K_s^0) and hyperons (Λ^0, Ξ^- and Ω^-) at various centralities from $Pb-Pb$ collisions at $\sqrt{s_{NN}}=2.76$ TeV [4, 5]. The yield of strange hadrons (with its anti-particle) obtained from $p-p$, $p-Pb$ and $Pb-Pb$ collisions are normalised with charged pions ($\pi^+ + \pi^-$) and displayed as a function of multiplicity in recent article [6]. Authors in [6] take the measurements of $Pb-Pb$ collisions (at $\sqrt{s_{NN}}=2.76$ TeV) from [4, 5] and $p-p$ collisions (at $\sqrt{s_{NN}}=7$ TeV) from [7–9] and $p-Pb$ collisions (at $\sqrt{s_{NN}}=5.02$ TeV) from [10]. The normalised yield of strange hadrons $(H_s + \bar{H}_s)/(\pi^+ + \pi^-)$, conveniently called as ‘*yield-ratio*’ show a smooth rising pattern with centrality (or multiplicity) for the hyperons and strange mesons following a saturation towards higher multiplicities. Observations from both *yield per participant* and *yield ratio* pose an important question regarding hyperon productions—whether the multistrange production yield is enhanced due to the increase in number density of constituent quarks or not?

Along this line, one more observation has been reported [11] where differences in production rates of strange and multistrange baryons have been observed in Au-Au compared to $p-p$ collisions at same energy, $\sqrt{s_{NN}}=200$ GeV.

* Correspondence email address: jajati-quark@vecc.gov.in

When the hyperon yields are scaled down by the number of participants (participating nucleons) an enhanced yield is observed relative to p+p collisions. The observed enhancement increases with the strangeness content of the hyperon, and that happens with centrality for all the hyperons.

In this article, we discuss hyperon productions at $\sqrt{s_{NN}}=200$ GeV, RHIC energy with a microscopic description using rate equation. We evaluate both *yield ratio* and *relative yield per participant* of hyperons for various centralities and compare with the observations from Au+Au collisions at midrapidity ($|\eta| < 0.5$)[3]. We also discuss the freeze out properties of strange hadrons by analyzing these two observables. From the analysis within the ambit of our model, we try to comment on the probable reason for more multi strange productions compared to single strange in central collisions .

As far as single strange hadron (K and Λ) productions are concerned, several literatures are available[1, 2, 12–23] in recent past, but these articles do not discuss multistrange productions. There are some literatures where the authors discuss subthreshold multistrange Ξ productions [24] with the inclusion of new resonance decay channels from massive baryons. A transport calculation on multistrange productions at SPS energy using ultra relativistic quantum molecular dynamics(UrQMD) is available [25]. Authors in [26, 27] use minimal statistical hadronisation model to explain NICA data. Present calculation adopts a microscopic approach and it discusses multi strange productions along with single strange hadrons at $\sqrt{s_{NN}}=200$ GeV, RHIC energy.

The manuscript is presented in the following manner. The rate equation for yield calculation is described in the Sec.II. Equations for hyperons and strange mesons along with evolution of the bulk is discussed in this section. The interactions of various hadronic species and their cross sections which tell about the microscopic origin of hyperon yields are considered in Sec.III. The rates of production are also described here. Due to expansion of the system, the temperature (T) and chemical potential (μ) of the bulk change with time. The evolution of T & μ are also described in this section. Theoretical estimation and its comparison with data are discussed in Sec.IV. Finally, we summarize in Sec.V with conclusion.

II. YIELD OF HYPERONS USING RATE EQUATION

There are several evidences which suggest that an initial hot-dense partonic system is produced in Au-Au collisions at RHIC at $\sqrt{s_{NN}}=200$ GeV[28–31]. It is also known by conventional wisdom that the hot-dense partonic system converts into hadronic system during the evolution as temperature falls below T_c . In the hadronic system, the hadrons change their numbers continuously due to rescatterings, till the chemical decoupling happens at a temperature T_{ch} , known as the chemical freeze-out temperature. At T_{ch} , the hadron yields get fixed and do not change subsequently. With subsequent colling, the hadrons decouple kinetically at a temperature T_{KF} , called as the knietic freeze-out temperature. After the knietic freeze-out, while particles stream freely towards the detector, some of the hadronic resonance states decay which is not a part of the rescattering effect of the medium. The chemical freeze-out temperatures may be same or different for different hadronic species. If T_{ch} is same for all species, then this is called as common freeze-out(chemical) temperature, and if T_{ch} is different for different species, then such a scenario can be described through sequential freeze-out mechanism. Sequential freeze-out is recently discussed in the following article [32]. Whether the freeze-out is common or sequential, it depends on the species of particle and the dynamical situation of the hadronic system.

To understand the probable freeze out scenario of hyperons and Kaons at RHIC energy, we here analyse the experimental observations by evaluating K, Λ, Ξ, Ω yield using rate equation or momentum intergated Boltzmann equation. We assume non-strange hadrons to provide a thermal background to the strange hadrons in the system. The use of rate equation is relevant here as the hadronic system produced in relativistic nuclear collisions at RHIC/LHC is supposed to be a dilute gas. Similar formalism has been used by us to explain the strange hadron production at LHC energy in [33]. Bjorken expansion is considered for the evolution of the bulk as it is relatively easier to analyze analytically. Again, our focus here, is to look at the ratio of the numbers (ratio of integrated yields) at freeze-out. The qualitative behaviour would be unchanged if we use 3-dimensional expansion to the present analysis. The value of freeze-out parametres may change. The results of the study of observables like flow and p_T spectra of identified hadrons would have been different with 3- and 1-dimensional expansion . A relevant 3-dimensional Hubble like expansion in hadronic phase is under progress to compare the results with Bjorken expansion and would be communicated later.

The complete set of rate equations for a system with hyperons, Λ, Ξ, Ω , and strange mesons, K, \bar{K} has been documented in Ref. [33]. We solve the same set of equations to analyze the strange hadron yields at RHIC for $\sqrt{s_{NN}}=200$ GeV. The set consists of first-order coupled ordinary differential equations which describe the time evolution of hadronic yields due to interactions within the system in presence of a dilution term due to expansion. The important inputs which are needed to solve the equations are the hadronic cross-sections, which are mentioned in the next section. To discuss the rate of production for a particular reaction, one may think of a channel $a + b \rightarrow c + d$ where the thermal average rate $\langle \sigma v \rangle_{ab \rightarrow cd}$ can be described as below. Assuming Maxwell-Boltzmann statistics for the particles, the reaction rate

TABLE I. Integrated yields of π [35] and K_s^0 [36] at midrapidity $|y| < 0.5$ for various centralities from Au+Au collisions at $\sqrt{s_{NN}}=200$ GeV which are used to calculate the *yield ratio* for K_s^0 and the same is tabulated here.

Centrality (%)	N_{part} [36]	dN/dy π^+ [35]	dN/dy π^- [35]	dN/dy K_s^0 [36]	$2K_s^0/(\pi^+ + \pi^-)$	K_s^0/N_{part}
0-5	350 \pm 4	322 \pm 25	327 \pm 25	43.5 \pm 2.4	0.134 \pm 0.0052	0.124 \pm 0.007
10-20	238 \pm 5	194 \pm 15	196 \pm 15	27.80 \pm 1.4	0.142 \pm 0.005	0.116 \pm 0.006
20-40	147 \pm 4	112.1 \pm 12.09	112.8 \pm 12.09	16.50 \pm 0.83	0.146 \pm 0.0066	0.112 \pm 0.006
40-60	67.5 \pm 2.7	47.5 \pm 5.25	47.6 \pm 5.30	7.26 \pm 0.49	0.152 \pm 0.007	0.107 \pm 0.008
60-80	23 \pm 1.2	15.9 \pm 1.79	16 \pm 1.79	2.14 \pm 0.19	0.134 \pm 0.007	0.093 \pm 0.009

TABLE II. Integrated yields of Λ, Ξ and Ω at midrapidity $|y| < 0.5$ for various centralities from Au+Au collisions at $\sqrt{s_{NN}}=200$ GeV are taken from [3]. The *yield ratio* for hyperons have been calculated and tabulated here.

Centrality (%)	N_{part} [3]	dN/dy Λ [3]	dN/dy $\bar{\Lambda}$ [3]	dN/dy Ξ^- [3]	dN/dy Ξ^+ [3]	dN/dy $\Omega^- + \Omega^+$ [3]	$\frac{(\Lambda+\bar{\Lambda})}{(\pi^++\pi^-)}$	$\frac{(\Xi^-+\Xi^+)}{(\pi^++\pi^-)}$	$\frac{(\Omega^-+\Omega^+)}{(\pi^++\pi^-)}$	$\frac{\Lambda+\bar{\Lambda}}{N_{part}}$	$\frac{\Xi^-+\Xi^+}{N_{part}}$	$\frac{\Omega^-+\Omega^+}{N_{part}}$
0-5	352 \pm 3	16.7 \pm 1.12	12.7 \pm 0.92	2.17 \pm 0.19	1.83 \pm 0.21	0.53 \pm 0.056	0.0453 \pm 0.003	0.0061 \pm 0.0005	0.00081 \pm 0.00009	0.0835 \pm 0.004	0.01136 \pm 0.0008	0.0015 \pm 0.00015
10-20	235 \pm 9	10.0 \pm 0.71	7.7 \pm 0.51	1.41 \pm 0.09	1.14 \pm 0.09	-	0.0454 \pm 0.003	0.0065 \pm 0.00048	-	0.0753 \pm 0.004	0.0108 \pm 0.0068	-
20-40	141 \pm 8	5.53 \pm 0.39	4.30 \pm 0.05	0.72 \pm 0.028	0.62 \pm 0.036	0.17 \pm 0.022	0.0437 \pm 0.0037	0.0059 \pm 0.0005	0.00075 \pm 0.00011	0.0697 \pm 0.0048	0.0095 \pm 0.0006	0.0012 \pm 0.00017
40-60	62 \pm 9	2.07 \pm 0.143	1.64 \pm 0.114	0.26 \pm 0.022	0.23 \pm 0.022	0.063 \pm 0.0089	0.039 \pm 0.0036	0.0051 \pm 0.0005	0.00066 \pm 0.0001	0.0598 \pm 0.009	0.0079 \pm 0.0012	0.0010 \pm 0.0002
60-80	21 \pm 6	0.58 \pm 0.041	0.48 \pm 0.032	0.063 \pm 0.005	0.061 \pm 0.0044	-	0.0331 \pm 0.003	0.0038 \pm 0.0003	-	0.05 \pm 0.014	0.0059 \pm 0.001	-

at a temperature T is given by [12, 34]

$$\langle \sigma v \rangle_{ab \rightarrow cd} = \frac{T^4}{4} \mathcal{C}_{ab}(T) \int_{z_0}^{\infty} dz [z^2 - (m_a/T + m_b/T)^2] \times [z^2 - (m_a/T - m_b/T)^2] \sigma K_1(z), \quad (1)$$

where

$$\mathcal{C}_{ab}(T) = \frac{1}{m_a^2 m_b^2 K_2(m_a/T) K_2(m_b/T)}.$$

Here σ and v respectively denote the scattering cross section and relative Möller velocity of incoming particles a and b for the process $a + b \rightarrow c + d$. K_2 is the modified bessel function of second kind. z is basically E/T , where E is the total centre of mass energy. The lower limit of the integration is $z_0 = \max(m_a + m_b, m_c + m_d)/T$. For a detailed derivation of the rate equations, one can see Appendix A in [33].

Unlike Hadron Resonance Gas model, we obtain the yield by solving the rate equations. We assume the initial densities to be slightly away from equilibrium. In this study, we do not consider the initial QGP phase. The initial number densities ($n_i(T_i)$, with T_i the initial temperature) of different hadrons can be constrained if the hadronization mechanism were known. Instead, we treat the initial number densities as parameters of the rate equations. Hence this calculation does not prohibit the initial QGP phase. Considering a Bjorken expansion of the hadronic medium, the temperature evolution is obtained numerically along with the rate equations. This is coded as Strange Hadron Transport in Heavy Ion Collision (SH-THIC). Evolution of baryonic chemical potential, μ_b , is also considered, even though μ_b is small (~ 25 MeV) at RHIC, $\sqrt{s_{NN}}=200$ GeV. Baryonic chemical potential is obtained from following equation for baryon number conservation:

$$\partial_\mu n_b^\mu = 0, \quad (2)$$

where $n_b^\mu = n_b u^\mu$ denotes the net-baryon density flow vector, and which is a function of T and μ_b . If the expansion is considered to be along the z -direction, then the flow velocity, u^μ , becomes $u^\mu = (\gamma, 0, 0, \gamma v_z)$. We adopt the following definition for the net-baryon density

$$n_b = \sum_{B=N,\Lambda,\Sigma,\Xi,\Omega} (n_B - n_{\bar{B}})$$

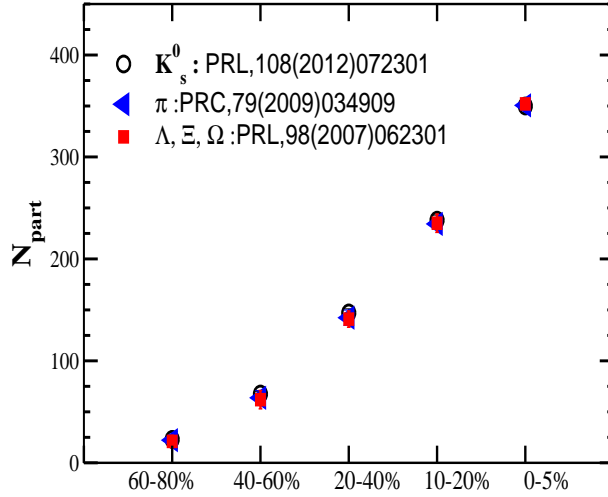


FIG. 1. N_{part} vs centrality as reported in three references [3, 35, 36].

and ignore the contribution from massive baryons above Δ mass. For the equation of state, we take $p = c_s^2 \epsilon$. Now using the energy-momentum conservation equation, $\partial_\mu T^{\mu\nu} = 0$ [37], we can obtain the temperature evolution as

$$T^{\frac{4}{(1+c_s^2)}} \tau = \text{constant}.$$

The initial baryon number densities n_b^i , time τ_i and temperature T_i are parameters. The hadronic system evolution starts from T_c .

III. SCATTERINGS OF HADRONS PRODUCING HYPERONS AND STRANGE MESONS AND CROSS SECTION OF VARIOUS PROCESSES.

Various scattering processes (along with inverse reaction) considered in our calculation to produce strange hadrons are:

$$\pi\pi \leftrightarrow K\bar{K}, \pi\rho \leftrightarrow K\bar{K}, \pi N \leftrightarrow \Lambda K, \pi\Lambda \leftrightarrow \bar{K}N, \pi\Sigma \leftrightarrow \bar{K}N, \pi\Xi \leftrightarrow \bar{K}\Lambda, \pi\Xi \leftrightarrow \bar{K}\Sigma, \rho\rho \leftrightarrow K\bar{K}, \rho N \leftrightarrow \Lambda K, \bar{K}N \leftrightarrow K\Xi, p\bar{p} \leftrightarrow K^- \bar{K}^+, p\bar{p} \leftrightarrow \Lambda\bar{\Lambda}, p\bar{p} \leftrightarrow \Sigma^- \bar{\Sigma}^+, p\bar{p} \leftrightarrow \Omega\bar{\Omega}, p\bar{p} \leftrightarrow \Xi\bar{\Xi}, \Lambda\Lambda \leftrightarrow N\Xi, \Lambda\Sigma \leftrightarrow N\Xi, \Sigma\Sigma \leftrightarrow N\Xi, \Lambda\bar{K} \leftrightarrow \Omega^- K^0, \Sigma^0 \bar{K} \leftrightarrow \Omega^- K^0.$$

The symbols take their as usual meaning. Isospin combinations are considered for all those processes where specific isospin channels are not mentioned. A few of the above processes, $YY \rightarrow N\Xi$, $\bar{K}N \rightarrow K\Xi$ and $\bar{K}Y \rightarrow \pi\Xi$, $\bar{K}N \rightarrow \pi Y$, although mentioned in literature, but are not considered due to unreasonable higher value of theoretical cross-sections, which are also not verified experimentally. In the above description, Y denotes either Λ or Σ hyperons. The details of the cross sections are mentioned in the appendix in a tabular form and also available in [33, 38]. The cross-sections for the inverse processes are calculated using the principle of detailed balance[39] as follows:

$$\sigma_{f \rightarrow i} = \frac{P_i^2}{P_f^2} \frac{g_i}{g_f} \sigma_{i \rightarrow f}, \quad (3)$$

where P_i, P_f are the momenta of incoming and outgoing channels in the center of mass frame, and g_i, g_f are the degeneracies, respectively. With above formalism the yields of strange hadrons, K, Λ, Ξ, Ω are calculated and presented in the next section.

IV. RESULTS

Taking cross sections as input, the number densities of K, Λ, Ξ, Ω are evaluated for various centralities through the rate equations. Then the densities are normalised with thermal pion densities. Initial number density, n_i , initial temperature, T_i and velocity of sound c_s are various parameters in this calculation. The hadron phase starts at T_c and

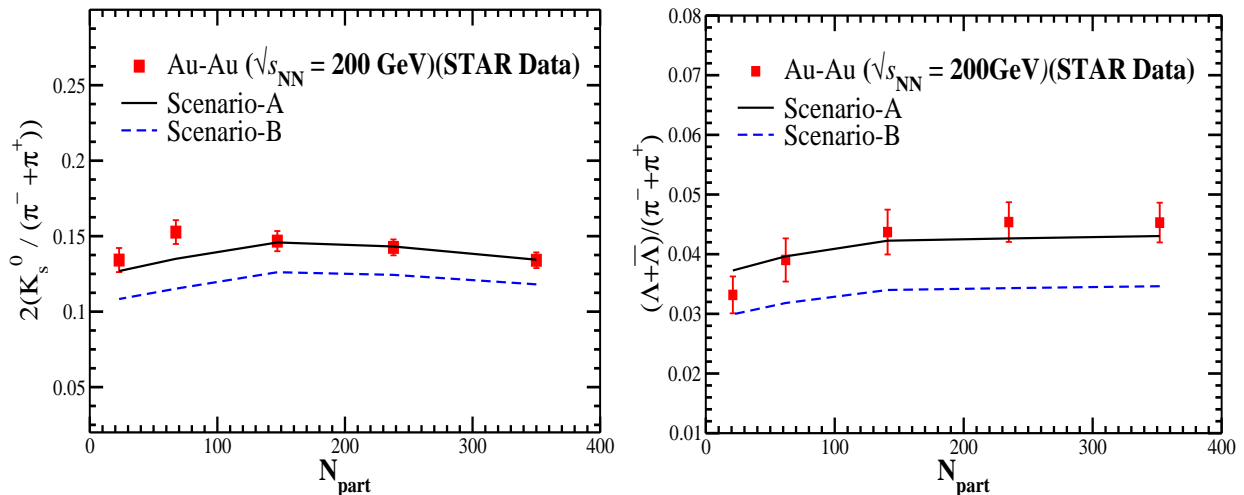


FIG. 2. Left panel: Yield ratio for K_s^0 from 200 GeV Au+Au collisions. Solid points with error bars represent data points measured by STAR Collaboration as reported in [36] and [35]. The solid line is the theoretical results. Right panel: Yield ratio for Λ from 200 GeV Au+Au collisions. Solid points with error bars represent data points measured by STAR Collaboration as reported in [3] and [35]. The solid line is the theoretical results.

the value is taken to be 156 MeV referring to the first principle QCD calculations based on lattice frame work [40]. We take $c_s^2=1/5$ for all cases. Different n_i and T_{ch} are taken for various scenarios to be discussed later.

Before presenting our theoretical results, we briefly discuss about the available data from Au-Au collisions at $\sqrt{s_{NN}} = 200$ GeV on *yield ratio* based on Ref. [3] and Ref. [36]. For K_s^0 , Λ , Ξ hadrons, mid rapidity data ($|\eta| < 0.5$) are available for five collision centralities; 0-5 %, 10-20 %, 20-40%, 40-60% and 60-80%. In case of Ω , the data are available in all those centralities apart from 10-20% and 60-80%. The p_T integrated yield, dN/dy , have been measured for Λ , $\bar{\Lambda}$, Ξ , $\bar{\Xi}$, Ω , $\bar{\Omega}$ in Ref. [3] and for K_s^0 in Ref. [36]. The rapidity windows for $\Lambda(\bar{\Lambda})$ is $|y| < 1$, for $\Xi^-(\bar{\Xi}^+)$ is $|y| < 0.75$ and for $\Omega^- + \Omega^+$ is $|y| < 0.75$. The intergated yield dN/dy is dominated by low p_T region of the spectra, that basically corresponds to soft production. dN/dy of pions from Au-Au collisons at same energy is measured in [35]. We take those experimental values and evaluate the ratios of the integrated yield of particles (plus anti-particles) to the pion yields, which are tabulated in the last columns of Tables- I & II . It may be reminded that there are minor differences in N_{part} values (at same centrality) in following references [3, 35, 36]. However the differences are very small as shown in Fig.1. We consider N_{part} from Ref. [3] in our calculation of *yield ratio* of hyperons. While calculating *yield ratio* of K_s^0 , we consider N_{part} from Ref. [36].

While evaluating the yield of Λ we have included contribution from Σ . Because we know it is difficult to isolate Λ^0 from Σ^0 , as Σ^0 decays to Λ^0 and γ through a weak process having 99% branching ratio. This makes the reconstruction of Σ^0 a difficult task. Hence, data of Λ contains Σ . The data takes into account the feed down corrections from Ξ , but not from Ω , $\Sigma^*(1385)$ family ($\Sigma^{+*}, \Sigma^{0*}, \Sigma^{-*}$) and $\Sigma^*(1660)$. In order to take care of the feed down contribution in our calculations, we multiply a constant factor 0.8 to the Λ yield.

The p_T window ($0.5 \text{ GeV} < p_T < 4.8 \text{ GeV}$) in which the data of integrated yields are presented covers the domain of soft productions which is within the scope of present theoretical calculation. We present the results in Fig.2 that displays the *yield ratio* of K_s^0 and Λ . We have considered $2K_s^0 = K^+ + K^-$. In both left and right panels, the solid points represent the data from Au-Au collisions by STAR Collaboration [3, 35, 36] and the solid curves are our numerical results. Initial number density is taken as $n_i=0.85n_{eq}$, where n_{eq} denotes the equilibrium density at T_i . This is described as scenario-A. We tabulate the values of T_{ch} in Table III that best explains the data in each centrality. We redo our calculations with different initial number density, $n_i = 0.7n_{eq}$, keeping T_{ch} same (Scenario B in Fig.2). The fitting is not well as it is displayed; the lowest data point is explained well (Λ) while the other points are underpredicted. We checked with other combination of parameters but the fitting is not good.

The *yield ratio* for multi-strange baryons, Ξ and Ω , are displayed in Fig.3 for both the scenarios A & B. The solid points of both panels represent the data from [3, 35], while the solid curves are our results with the same initial conditions considered to explain K_s^0 and Λ in Fig.2. Scenario-A with $n_i = 0.85n_{eq}$ explains the data points nicely except for the most peripheral one (having centrality, 60-80 %). In case of Ω the datum point is not available for 60-80% centrality, but it is also expected that scenario A would over-predict. However, a lower initial number density ($n_i < 0.7n_{eq}$) is observed to explain Ξ, Ω yield ratio at most peripheral collsion, which is also expected from scenario B. Here also, we observe a step rise in the *yield ratio*, when we move from (60-80)% centrality to (20-40)% centrality. For both

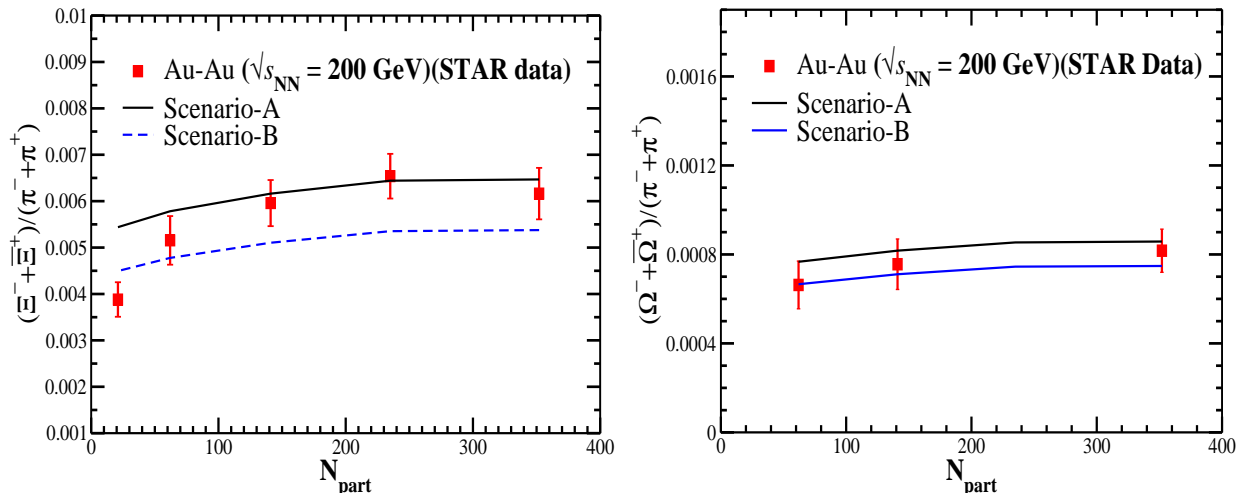


FIG. 3. Left panel: Yield ratio for Ξ from 200 GeV Au+Au collisions. Solid points with error bars represent data points measured by STAR Collaboration. The solid line is the theoretical results. Right panel: Yield ratio for Ω from 200 GeV Au+Au collisions. Solid points with error bars represent data points measured by STAR Collaboration. The solid line is the theoretical results. Data are taken from [3] and [35]

TABLE III. Parameters with freeze-out temperature (T_{ch} , that explains the data. Reference Figs.2,3,4.

N_{part}	C_s^{-2}	$T_{ch}(K_s^0)$ (in GeV)	$T_{ch}(\Lambda)$ (in GeV)	$T_{ch}(\Xi)$ (in GeV)	$T_{ch}(\Omega)$ (in GeV)
352	1/5	148.3	152	154.5	155
235	1/5	149.3	151	154.2	*
141	1/5	149.2	150	150	150.19
62	1/5	144.5	144.5	144.5	145
21	1/5	139	139	139	*

scenarios, A and B, the T_{ch} are kept same as mentioned in Table-III. One can explore other scenarios with different initial conditions. Similar analysis has been carried out by us while explaining the data at LHC [33] at a different collision energy. From the analysis at both colliding energies we find a similar trend *i.e.*, lower initial densities explain better the most peripheral collisions. This is expected as a system with smaller energy densities might be produced at most peripheral collisions; which produce less particle densities.

Let's discuss the other observable, relative yield of strange hadrons. It may be noted that the enhancement of multi strange productions is highlighted in [3] by measuring the relative yield. It is basically the normalized yield in central collision to the normalized yield at most peripheral collision. The yield is normalized with N_{part} . The relative yield is written as $dN/dy/N_{part}$ ($= ((dN/dy)/N_{part})_{centrality} / ((dN/dy)/N_{part})_{mostperipheral}$). When the comparison of relative yield is made for multistrange (Ξ^+) anti hyperon with single strange (Λ) anti hyperon, then it is observed the value of the relative yield is more for multi strange compared to the single strange hadron. The values of the *relative yields* of anti-hyperons $\bar{\Lambda}$ and $\bar{\Xi}^+$ are tabulated in Table IV. Fig.4 shows the relative yield per participant with N_{part} . The relative yield per participant is presented with respect to most peripheral collisions *i.e.*, centrality (60-80)%. In a particular centrality class x , relative yield is $(dN/dy)/N_{part} = [(dN/dy)/N_{part}]_x / [(dN/dy)/N_{part}]_{60-80\%}$ [3]. The blue

TABLE IV. Relative yield of anti-hyperons per participant at various centralities (with respect to most peripheral collision) from Au+Au collisions at $\sqrt{s_{NN}}=200$ GeV. Relative $(dN/dy)/N_{part} = \frac{[(dN/dy)/N_{part}]_x}{[(dN/dy)/N_{part}]_{60-80\%}}$, where x represents centrality.

Centrality %	N_{part}	Relative $(dN/dy)/N_{part}$ (Λ)	Relative $(dN/dy)/N_{part}$ ($\bar{\Xi}^+$)
0-5	352 ± 3	1.578 ± 0.476	1.7897 ± 0.565
10-20	235 ± 9	1.433 ± 0.434	1.67 ± 0.513
20-40	141 ± 8	1.334 ± 0.398	1.513 ± 0.463
40-60	62 ± 9	1.157 ± 0.387	1.277 ± 0.437
60-80	21 ± 6	1.0 ± 0.414	1.0 ± 0.417

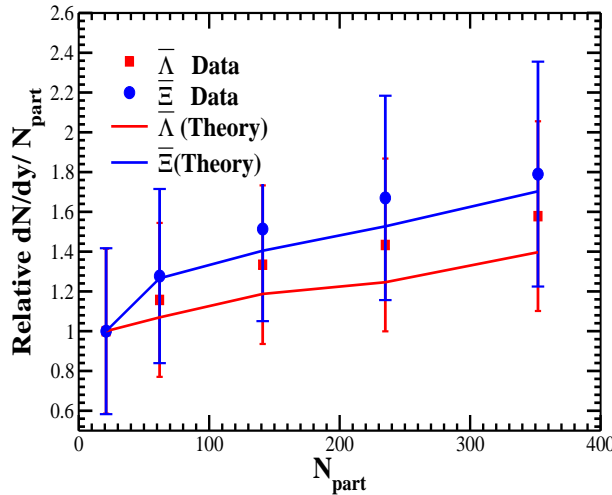


FIG. 4. Relative $dN/dy/N_{part}$ is basically the ratio of yield/ N_{part} at certain centrality to the yield/ N_{part} at most peripheral(60-80%). The red color is for the $\bar{\Lambda}$ and blue for $\bar{\Xi}$ hyperons. The error bar includes both statistical and systematic.

solid points are data points for $\bar{\Xi}$ and red points are for $\bar{\Lambda}$. Solid lines are numerical results. It is worth to mention here, that the data we consider from [3] (Fig.2 of the paper) displays the statistical error bars only. Here we consider both statistical and systematic error. Both for $\bar{\Lambda}$ and $\bar{\Xi}$, there is an increase in yield per participant in central collisions compared to peripheral collisions. The increase is more in case of $\bar{\Xi}$ compared to $\bar{\Lambda}$.

The freeze-out temperatures(T_{ch}) considered in our calculation to explain simultaneously the *yield ratio* in Figs.2,3 and *relative yields* 4 are plotted in Fig.5. In case of central collisions, multi strange hadrons Ξ, Ω freeze out at a temperature close to very close to T_c . Λ freezes out little later. K_s^0 freezes out later. In peripheral collisions all freeze out simultaneously showing a common freeze-out temperature. It is also observed that T_{ch} decreases with N_{part} .

V. SUMMARY AND CONCLUSIONS

Multi strange productions from Au+Au collisions at $\sqrt{s_{NN}}=200$ GeV have been discussed microscopically using rate equations considering the cross sections of various hadronic processes. Rate equations are solved simultaneously both for single strange K, Λ, Σ and multi strange Ξ and Ω hadrons. The yield of strange hadrons with their anti-particles are normalised with thermal pions to get the *yield ratios*, such as, $(K^+ + K^-)/(\pi^+ + \pi^-)$, $(\Lambda + \bar{\Lambda})/(\pi^+ + \pi^-)$, $(\Xi^- + \Xi^+)/(\pi^+ + \pi^-)$ and $(\Omega^- + \Omega^+)/(\pi^+ + \pi^-)$ at various centralities. The results are then compared with the experimental data from Refs. [3, 36]. The *yield per participant* for anti-hyperons $\bar{\Xi}, \bar{\Lambda}$ are also evaluated for various N_{part} and compared with experimental observations. The freeze out temperatures are also extracted for various centrality of collisions. From the results of *yield ratios* of K_s^0, Λ, Ξ and Ω , it has been observed that the data are explained satisfactorily with $n_i = 0.85n_{eq}$ for central collisions where N_{part} is large. For most peripheral collisions, the hyperon productions are not well explained with $n_i = 0.85n_{eq}$, rather these are explained with less initial densities, $n_i = 0.7n_{eq}$. A lower value of initial number density in most peripheral collision may indicate that less initial energy densities are created in most peripheral collisions due to less number of participating nucleons, as expected.

The rise of *yield ratios* with N_{part} is observed for all strange hadrons which indicates the increase in strangeness production with centrality. Large steepness is seen in case of multi-strange hadrons compared to K and Λ . This tells about the enhancement of multistrange production rate. This probably says that the probability of formation of multistrange hadrons from the bulk increases with N_{part} due to increase in number of interactions. It may also be argued in another way, that there is an increase in the rate of more massive hadron productions with centrality (as steepness is more for heavier Cascade compared to Kaon and Lambda), indicating some sort of mass ordering.

The above argument is again more pronounced from the observation of *yield per participant* with N_{part} . There is a systematic increase in the *yield per participant* with N_{part} as one moves from lighter proton to heavier Cascade [3]. Instead of attributing this phenomenon to an increase in the number of initial constituents, this may be attributed to mass ordering. However, the R_{CP} measurements of Λ, Ξ, Ω with p_T in [3] discards the reason related to mass, but attribute the same to the constituent quarks, the density of which increases with centrality. In this theoretical calculation, we observed an increase in initial number densities of strange hadrons from most peripheral ($n_i = 0.7n_{eq}$) to central ($0.8n_{eq}$) collisions, which is required to explain the data. Initial number densities are parameteres in this study, but in principle should be constrained from strange quark densities assuming an initial QGP phase. This is kept

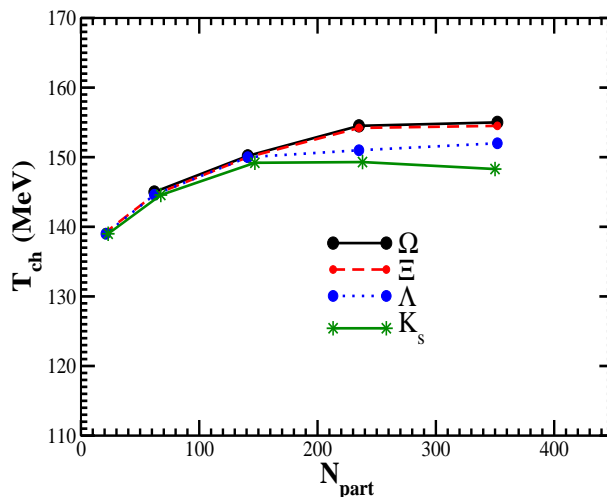


FIG. 5. The corresponding T_{ch} for hyperons and strange mesons, that explain the above data.

for a future work.

The *relative yield per participant* basically tells about the scaling property of baryons(anti baryons) with centrality. Here it is shown by considering anti-baryons $\bar{\Lambda}$ and $\bar{\Xi}$. Strange anti-baryons are chosen as scaling observables because the valence quark content of these particles can only be created in the collisions. Hence, the information from this observable can shed light on the produced system. Even if one considers the *relative yield per participant* with strange baryons, the inference would be similar at this colliding energy. This is because baryon to anti-baryon ratio is close to one at such high energy collisions. The analysis is done only for $\bar{\Lambda}$ and $\bar{\Xi}$ as data of $\bar{\Omega}$ are not available.

It may be pointed out that similar behaviour of *yield ratio*, $(H_s + \bar{H}_s)/(\pi^+ + \pi^-)$ is observed from Pb-Pb collisions at $\sqrt{s_{NN}}=2.76$ TeV, LHC energy [33]. The multi-strange data at most peripheral collision are over predicted when n_i for both central collision and most peripheral collision are considered same. The system that is produced in most peripheral collisions may be far away from thermodynamic equilibrium and should not be treated at par with most central collisions at RHIC, $\sqrt{s_{NN}}=200$ GeV, and at LHC, $\sqrt{s_{NN}}=2.76$ TeV. While moving from most peripheral to central collisions, when a smooth behaviour of the *yield ratio* is obtained instead of steep rise, one probably expect a change in the medium property. Now question arises, whether the change in medium property can be attributed to (i) the presence or absence of initial partonic system or (ii) presence of initial partonic system but with less or more strange parton density? It is a matter of future investigation.

The freeze-out temperatures obtained within the ambit of this present calculation signify a sequential freeze out for multi strange & single strange hadrons in case of central collisions and a common freeze out for all in most peripheral collisions. Multi strange Ξ, Ω freeze out at a temperature very close to T_c . It is also observed that T_{ch} decreases with N_{part} .

Appendix: Cross-section

The cross sections for various hadronic processes producing hyperons and strange mesons are listed below along with corresponding references. The cross-sections of all inverse reactions are obtained using principle of detailed balance as follows; $\sigma_{f \rightarrow i} = \frac{P_i^2}{P_f^2} \frac{g_i}{g_f} \sigma_{i \rightarrow f}$ where P_i, P_f are the center of mass momenta and g_i, g_f are the total degeneracies of the initial and final channels.

TABLE V. Cross sections for K, Λ, Σ production

Reaction	Cross-section	Remarks
$\pi\pi \rightarrow K\bar{K}$ [41] $\rho\rho \rightarrow K\bar{K}$ $\pi\rho \rightarrow K\bar{K}^*$ $\pi\rho \rightarrow K^*\bar{K}$	$\bar{\sigma}_{ab \rightarrow cd}(s) = \frac{1}{32\pi} \frac{P'_{cd}}{sP'_{ab}} \int_{-1}^1 dx M(s, x)$	P_{ab}, P'_{cd} - three momenta of incoming mesons and outgoing Kaons in the CM frame, $x = \cos(P_{ab}, P'_{cd})$. $M(s, x)$ is the invariant amplitude calculated using following interaction Lagrangian densities [41] $\mathcal{L}_{K^*K\pi} = g_{K^*K\pi} K^{*\mu} \tau [K(\partial_\mu \pi) - (\partial_\mu K)\pi]$ $\mathcal{L}_{\rho KK} = g_{\rho KK} [K\tau(\partial_\mu K) - (\partial^\mu K)\tau K]\rho^\mu$
$\pi N \rightarrow \Lambda K$ [41, 42] $\pi N \rightarrow \Sigma K$ $\rho N \rightarrow \Lambda K$ $\rho N \rightarrow \Sigma K$	$\bar{\sigma}_{MB \rightarrow YK} = \sum_i \frac{(2J_i+1)}{(2S_1+1)(2S_2+1)} \frac{4\pi}{k_i^2} \frac{\Gamma_i^2/4}{(\sqrt{s}-m_i)^2 + \Gamma_i^2/4} B_i^{\text{in}} B_i^{\text{out}}$ <p>Here M and B stands for Meson and Baryon resp. Y stands for Λ or Σ</p>	The sum is over resonances with mass(m_i), spin (J_i) and decay width(Γ_i). $N_1^*(1650)$, $N_2^*(1710)$, $N_3^*(1720)$ [43] and $N_5^*(1875)$, $N_6^*(1900)$ [44] are considered as intermediate resonant states. $(2S_1 + 1)$ and $(2S_2 + 1)$ are the polarisation states of the meson (M) and baryon(B) in the incoming channels. B_i represents the branching ratio.
$\bar{K}N \rightarrow \Sigma\pi$ [45, 46]	$\sigma_{\bar{K}N \rightarrow \Sigma\pi} = \sigma_{K^-p \rightarrow \Sigma^0\pi^0} + \sigma_{K^-n \rightarrow \Sigma^0\pi^-},$ <p>where $\sigma_{K^-p \rightarrow \Sigma^0\pi^0} \approx \sigma_{K^-n \rightarrow \Sigma^0\pi^-}$ and</p> $\sigma_{K^-p \rightarrow \Sigma^0\pi^0} = \begin{cases} 0.624 p^{-1.83} \text{ mb} & \text{if } p \leq 0.345 \text{ GeV} \\ \frac{0.0138}{(p-0.385)^2 + 0.0017} \text{ mb} & \text{if } 0.345 < p \leq 0.425 \text{ GeV} \\ 0.7 p^{-2.09} \text{ mb} & \text{if } p > 0.425 \text{ GeV} \end{cases}$	p is the anti-Kaon momentum in the Lab frame
$\bar{K}N \rightarrow \Lambda\pi$ [45, 46]	$\sigma_{K^-p \rightarrow \Lambda\pi^0} = \begin{cases} 1.205 p^{-1.428} \text{ mb} & \text{if } p \geq 0.6 \text{ GeV} \\ 3.5 p^{0.659} \text{ mb} & \text{if } 0.6 < p \leq 1.0 \text{ GeV} \\ 3.5 p^{-3.97} \text{ mb} & \text{if } p > 1.0 \text{ GeV} \end{cases}$	p is the anti-Kaon momentum in the Lab frame
$pp \rightarrow K\bar{K}$ [47–49] $pp \rightarrow \Lambda\bar{\Lambda}$ $pp \rightarrow \Sigma\bar{\Sigma}$	$\sigma_{P\bar{P} \rightarrow \bar{Y}Y(K\bar{K})} = \frac{C_A C_{Y_i(K)} g_0^4}{16\pi} \times \frac{s}{s-4m_P^2} \times \Gamma(1 - \alpha(0))^2 \times \left(\frac{s}{s_0} \right)^{2(\alpha_0-1)} \times \frac{e^{A_1 t_{\text{min}}}}{\Lambda_1}$	Refer Table VIII for values of parameters.

TABLE VI. Cross sections for Ξ production

Reaction	Cross-section	Remarks
$\bar{K}\Lambda \rightarrow \pi\Xi$ [50, 51]	$\sigma_{\bar{K}\Lambda \rightarrow \pi\Xi} = \frac{1}{4} \frac{p_\pi}{p_{\bar{K}}} M_{\bar{K}\Lambda \rightarrow \pi\Xi} ^2$ with $ M_{\bar{K}\Lambda \rightarrow \pi\Xi} ^2 = 34.7 \frac{s_0}{s}$	p_π and p_K - momentum in CM frame $s_0 = \sum_i m_i$ - threshold energy
$\bar{K}\Sigma \rightarrow \pi\Xi$ [50, 51]	$\sigma_{\bar{K}\Sigma \rightarrow \pi\Xi} = \frac{1}{12} \frac{p_\pi}{p_{\bar{K}}} M_{\bar{K}\Sigma \rightarrow \pi\Xi} ^2$ with $ M_{\bar{K}\Sigma \rightarrow \pi\Xi} ^2 = 318 \left(1 - \frac{s_0}{s}\right)^{0.6} \times \left(\frac{s_0}{s}\right)^{1.7}$	p_π and p_K - momentum in CM frame $s_0 = \sum_i m_i$ - threshold energy
$\Lambda\Lambda \rightarrow N\Xi$ [52-54]	$\sigma_{\Lambda\Lambda \rightarrow N\Xi} = 37.15 \frac{p_N}{p_\Lambda} (\sqrt{s} - \sqrt{s_0})^{-0.16}$ mb	Parametrisation valid for $0 < (\sqrt{s} - \sqrt{s_0}) < 0.6$ GeV
$\Lambda\Sigma \rightarrow N\Xi$ [52-54]	$\sigma_{\Lambda\Sigma \rightarrow N\Xi} = 25.12 (\sqrt{s} - \sqrt{s_0})^{-0.42}$ mb	Parametrisation valid for $0 < (\sqrt{s} - \sqrt{s_0}) < 0.6$ GeV
$\Sigma\Sigma \rightarrow N\Xi$ [52-54]	$\sigma_{\Sigma\Sigma \rightarrow N\Xi} = 8.51 (\sqrt{s} - \sqrt{s_0})^{-0.395}$ mb	Parametrisation valid for $0 < (\sqrt{s} - \sqrt{s_0}) < 0.6$ GeV
$\bar{K}N \rightarrow K\Xi$ [52-55]	$\sigma_{\bar{K}N \rightarrow K\Xi} =$ $0.5 [\sigma_{K^-p \rightarrow K^+\Xi^-} + \sigma_{K^-p \rightarrow K^0\Xi^0} + \sigma_{K^-n \rightarrow K^0\Xi^-}]$ with $\sigma_{K^-p \rightarrow K^+\Xi^-} = 235.6 \left(1 - \frac{\sqrt{s_0}}{\sqrt{s}}\right)^{2.4} \left(\frac{\sqrt{s_0}}{\sqrt{s}}\right)^{16.6}$ mb $\sigma_{K^-p \rightarrow K^0\Xi^0} = 7739.9 \left(1 - \frac{\sqrt{s_0}}{\sqrt{s}}\right)^{3.8} \left(\frac{\sqrt{s_0}}{\sqrt{s}}\right)^{26.5}$ mb $\sigma_{K^-n \rightarrow K^0\Xi^-} = 235.6 \left(1 - \frac{\sqrt{s_0}}{\sqrt{s}}\right)^{2.4} \left(\frac{\sqrt{s_0}}{\sqrt{s}}\right)^{16.6}$ mb	Parametrisation valid for $0 < (\sqrt{s} - \sqrt{s_0}) < 1$ GeV
$\bar{p}p \rightarrow \bar{\Xi}^0\Xi^0$ [47]	$\sigma_{\bar{p}p \rightarrow \bar{\Xi}^0\Xi^0} = \frac{16}{81\pi} \frac{[\sigma_{\bar{p}p \rightarrow \bar{\Lambda}\Lambda}]^2}{2\Lambda_1} \exp[\Lambda_1 t_{DO}]$ Here $\Lambda_1 = 9 \text{ GeV}^{-2}$	Refer Table V for $\sigma_{\bar{p}p \rightarrow \bar{\Lambda}\Lambda}$
$\bar{p}p \rightarrow \bar{\Xi}^+\Xi^-$ [47]	$\sigma_{\bar{p}p \rightarrow \bar{\Xi}^+\Xi^-} = 16\sigma_{\bar{p}p \rightarrow \bar{\Xi}^0\Xi^0}$	

TABLE VII. Cross sections for Ω production

Reaction	Cross-section	Remarks
$K^-\Lambda \rightarrow \Omega^-K^0$ [38, 56]	$\sigma_{K^-\Lambda \rightarrow \Omega^-K^0} = a_0 + a_1 p_{\text{lab}} + a_2 p_{\text{lab}}^2 + a_3 \exp(-a_4 p_{\text{lab}})$ $1.011 \leq p_{\text{lab}}(\text{GeV}) \leq 6.55$	$a_0 = 0.155591, a_1 = -0.0473326,$ $a_2 = 0.00362302$ $a_3 = -0.29776, a_4 = 0.917116$
$K^-\Sigma^0 \rightarrow \Omega^-K^0$ [38, 56]	$\sigma_{K^-\Sigma^0 \rightarrow \Omega^-K^0} = b_0 + b_1 p_{\text{lab}} + b_2 p_{\text{lab}}^2 + b_3 \exp(-b_4 p_{\text{lab}})$ $1.19 \leq p_{\text{lab}}(\text{GeV}) \leq 5.991$	$b_0 = 0.137027, b_1 = -0.0422865,$ $b_2 = 0.00327658$ $b_3 = -0.281588, b_4 = 0.942457$
$\pi^0\Xi^- \rightarrow \Omega^-K^0$ [38, 56]	$\sigma_{\pi^0\Xi^- \rightarrow \Omega^-K^0} = c_0 + c_1 p_{\text{lab}} + c_2 p_{\text{lab}}^2 + c_3/p_{\text{lab}} +$ $c_4/(p_{\text{lab}}^2) + c_5 \exp(-p_{\text{lab}})$ $1.033 \leq p_{\text{lab}}(\text{GeV}) \leq 5.351$	$c_0 = -0.414988, c_1 = -0.025499,$ $c_2 = 0.00628967$ $c_3 = 2.1816, c_4 = -0.639193,$ $c_5 = -2.85555$
$\bar{p}p \rightarrow \Omega^-\bar{\Omega}^+$ [47]	$\sigma_{\bar{p}p \rightarrow \Omega^-\bar{\Omega}^+} = \frac{4^3}{\pi^2} \times \frac{[\sigma_{\bar{p}p \rightarrow \bar{\Lambda}\Lambda}]^3}{\Lambda_1^3} \times \exp[\Lambda_1 t_{DO}]$	$t_{DO} = t_{min}^{\Lambda\Xi} - t_{min}^{\Lambda} + t_{min}^{\Xi\Omega} - t_{min}^{\Lambda}$ with $t_{min}^{ij} =$ $-\frac{s}{2} + m_i^2 + m_j^2 + \frac{1}{2} \sqrt{(s - 4m_i^2)(s - 4m_j^2)}$ Refer Table V for $\sigma_{\bar{p}p \rightarrow \bar{\Lambda}\Lambda}$

TABLE VIII. Parameters for $pp \rightarrow YY(MM)$ Reactions[57-61]

Reactions	C_A	$C_{Y_i(M_i)}(\text{GeV}^{-2})$	$\Lambda_1(\text{GeV}^2)$	s_0	Regge trajectory $\alpha(t) =$
$pp \rightarrow K^+K^-$	0.08	4	4	1.93	$-0.86+0.5t$
$pp \rightarrow \Lambda\Lambda$	0.10	9/4	9	2.43	$0.32+0.85t$
$pp \rightarrow \Sigma^-\Sigma^+$	0.10	1	9	2.43	$0.32+0.85t$

-
- [1] M. Gazdzicki, J. Phys. G **30**, S701(2004).
- [2] J. Rafelski and B. Muller, Phys. Rev. Lett **48**, 1066(1982).
- [3] J. Adam *et al.*, Phys. Rev. Lett. **98**, 062301(2007).
- [4] B. Abelev *et al.* for ALICE Collaboration, Phys. Lett. B **728**, 216(2014).
- [5] B. Abelev *et al.* for ALICE Collaboration Phys. Rev. Lett. **111** (2013)222301.
- [6] J. Adam *et al.*, for ALICE Collaboration, Nat. Phys. **13**, 535-539(2017).
- [7] B. Abelev *et al.* ALICE Collaboration, Phys. Lett. B **712**, 309318(2012).
- [8] S. Acharya *et al.*, ALICE Collaboration, Phys. Rev. C **99**, 024906(2019).
- [9] Gyula Benczeri on behalf of ALICE Collaboration, arxiv:hep-ex-1801.03350.
- [10] J Adam *et al.* for ALICE Collaboration, arXiv:1512.07227 (2016).
- [11] J. Adams *et al.* for STAR Collaboration, Phys. Rev. C **77**, 044908(2008).
- [12] J. Kapusta and A. Mekjian, Phys. Rev. D **33**, 1304(1986).
- [13] J. Cugnon, P. Deneye and J. Vandermeulen, Phys. Rev. C **41**, 1701(1990).
- [14] J. Letessier and J. Rafelski, Eur. Phys. J. A **35**, 221(2008).
- [15] J. Rafelski and J. Letessier, Acta Phys. Polon. B **30**, 3559(1999).
- [16] B. Tomasik and E. E. Kolomeitsev, Eur. Phys. J. C **49**, 115 (2007); B. Tomasik, nucl-th/0509101.
- [17] S. Chatterjee, R. M. Godbole and Sourendu Gupta, Phys. Rev. C **81**, 044907 (2010).
- [18] J. Cleymans, H. Oeschler, K. Redlich and S. Wheaton, hep-ph/0510283.
- [19] A. Andronic, P. Braun-Munzinger and J. Stachel, Nucl. Phys. A, **772**(2006)167; Erratum ibid **678**, 516 (2009).
- [20] Jajati K. Nayak, J. Alam, B. Mohanty, P. Roy and A. K. Dutt-Mazumder, Acta Phys.Slov. **56**, 27 (2006).
- [21] Jajati K. Nayak, S. Banik and J. Alam, Phys. Rev. C **82**, 024914 (2010).
- [22] A. Tawfik, Fizika B **18**, 141 (2009).
- [23] Jajati K. Nayak, Sarmistha Banik and Jan-e Alam, Nucl. Phys. A **862–863**,286–289 (2011) <https://doi.org/10.1016/j.nuclphysa.2011.06.001>
- [24] J Steinheimer and M Bleicher, J. Phys. G **43**, (2016)015104.
- [25] S. Soff, S. A. Bass, M. Bleicher, L. Bravina and E. Zabrodin, H. Stöcker, W. Greiner, Phys. Lett. B **471**, (1999)89.
- [26] E. E. Kolomeitsev, B. Tomasik and D. N. Voskresensky, Phys. Rev. C **86**, 054909 (2012).
- [27] B. Tomasik and E. E. Kolomeitsev, Eur. Phys. J. A doi:10.1140/epja/i2016-16251-6 [arXiv:1510.04349(2015)].
- [28] I. Arsene *et al.*, "Quark–gluon plasma and color glass condensate at RHIC? The perspective from the BRAHMS experiment-perspective on discoveries at RHIC". Nuclear Physics A. 757 (2005)1–27.
- [29] B. B. Back *et al.*, "The PHOBOS perspective on discoveries at RHIC". Nuclear Physics A. 757 (2005)28–101.
- [30] J. Adams *et al.*, "Experimental and theoretical challenges in the search for the quark–gluon plasma: The STAR Collaboration’s critical assessment of the evidence from RHIC collisions". Nucl. Phys. A. 757 (2005): 102–183.
- [31] K. Adcox *et al.* (2005). "Formation of dense partonic matter in relativistic nucleus–nucleus collisions at RHIC: Experimental evaluation by the PHENIX Collaboration". Nucl. Phys. A. **757**, (2005) 184–283.
- [32] Rene Bellewied, EPJ Web of Conferences 171, 02006 (2018);doi.org/10.1051/epjconf/201817102006;J. Noronha-Hostler *et al.*, PoS, **347** (2019)175. <https://doi.org/10.22323/1.347.0175>
- [33] Purabi Ghosh, Jajati K. Nayak, Sushant Singh and Santosh K. Agarwalla, Phys. Rev. D**101**, 094004(2020).
- [34] P. Gondolo and G. Gelmini, Nucl. Phys. B**360**, 145-179(1991).
- [35] B. Abelev *et al.* for STAR Collaboration, Phys. Rev. C **79**, 034909(2009).
- [36] G. Agakishiev *et al.*, for STAR Collaboration, Phys. Rev. Lett. **108**, 072301(2010).
- [37] J. D. Bjorken, Phys. Rev. D, **27**,140(1983).
- [38] Purabi Ghosh, Jajati K. Nayak, Sushant K. Singh and Santosh Kumar Agarwala, arXiv:1906.11115.
- [39] J. Cugnon *et al.* Lettere Al Nuvo Cemento **41** 213(1984).
- [40] A. Bazavov *et al.*, Phys. Rev. D **95**(2017) 054504.
- [41] G. E. Brown *et al.* Phys. Rev. C **43**, 1881(1991).
- [42] J. Cugnon, R. M. Lombard, Nucl. Phys. A **422**,635(1984).
- [43] C. Amslar *et al.* Phys. Lett. B **667**(2008) 1.
- [44] C. Patrignani *et al.* (PDG), Chin. Phys. C **40**(2016) 100001.
- [45] G. Q. Li, C. -H. Lee, G. E. Brown Nucl. Phys. A **625**(1997)372.
- [46] C. M. Ko, Phys. Lett. B **120**(1983)294.
- [47] A. B. Kaidalov, P. E. Volkovitsky, Z.Phys.C **63**,517(1994).
- [48] A.I.Titov,B.Kampfer,Physical Reveiw C **78**,025201(2008).
- [49] K. G. Boreskov and A. B. Kaidalov, Sov. J. Nucl. Phys. 37, 100(1983); [Yad. Fiz. 37, 174 (1983).
- [50] L. W. Chen, C. M. Ko, Y. H. Zheng, Phys. Lett. B **584**, 269 (2004).
- [51] C. H. Li, C. M. Ko, Nucl. Phys. A **712** (2002) 110.
- [52] F. Li, L. Chen, C. M. Ko and S. H. Lee, Phys. Rev. C **85**, 064902(2012).
- [53] B. Holzenkamp, K. Holinda, J. Speth, Nucl. Phys. A **500** (1989) 485.
- [54] R. A. Adelseck, B. Saghai, Phys. Rev. C **42** (1990)108.
- [55] D. A. Sharov, V. L. Krotkikh, and D. E. Lanskoj, Eur. Phys. J. A **47**, 109 (2011).
- [56] T. Gaitanos *et al.*, Nucl. Phys. A **954** , 308(2016).

- [57] F. Flaminio *et al.*; preprint CERN-HERA 84-01(1984).
- [58] P. D. Barnes *et al.*, Phys. Lett. **189 B**(1987)249; *ibid.*229B(1989) 432;*ibid.***246B**(1990)237; Nucl. Phys.A **526** (1991) 575.
- [59] A. Hasan *etal.*, Nucl. Phys. B **378** (1992)3.
- [60] T. Tanimori *et al.* phys. Rev. D **41**(1990)744; Phys. Rev. Lett. **55** (1985)1835.
- [61] Y. Sugimoto *et al.* Phys. Rev. D **37** (1988) 583.